JMEPEG (2012) 21:2407–2416
DOI: 10.1007/s11665-012-0168-5

1059-9495/$19.00

Thermal Behavior of Mechanically Alloyed Powders Used for Producing an Fe-Mn-Si-Cr-Ni Shape Memory Alloy

B. Pricop, U. Söyler, N.M. Lohan, B. Özkal, L.G. Bujoreanu, D. Chicet, and C. Munteanu

(Submitted September 27, 2011)

In order to produce shape memory rings for constrained-recovery pipe couplings, from Fe-14 Mn-6 Si-9 Cr-5 Ni (mass%) powders, the main technological steps were (i) mechanical alloying, (ii) sintering, (iii) hot rolling, (iv) hot-shape setting, and (v) thermomechanical training. The article generally describes, within its experimental-procedure section, the last four technological steps of this process the primary purpose of which has been to accurately control both chemical composition and the grain size of shape memory rings. Details of the results obtained in the first technological step, on raw powders employed both in an initial commercial state and in a mixture state of commercial and mechanically alloyed (MA) powders, which were subjected to several heating-cooling cycles have been reported and discussed. By means of differential scanning calorimetry (DSC), scanning electron microscopy (SEM), and X-ray diffraction (XRD), the thermal behaviors of the two sample powders have been analyzed. The effects of the heating-cooling cycles, on raw commercial powders and on 50% MA powders, respectively, were argued from the point of view of specific temperatures and heat variations, of elemental diffusion after thermal cycling and of crystallographic parameters, determined by DSC, SEM, and XRD, respectively.

Keywords Fe-Mn-Si shape memory alloys, magnetic transition, mechanical alloying, powder metallurgy, thermal behavior

1. Introduction

Shape memory alloys (SMAs) are the functional materials which can recover from being deformed when heated (Ref 1). There are three major types of commercial SMA systems at present, namely, Cu-based (mainly Cu-Al-Ni and Cu-Zn-Al), Ni-Ti-based, and Fe-based (e.g., Fe-Mn-Si, Fe-Ni-C and Fe-Ni-Co-Ti) (Ref 2). Since they are cheaper and easier to process (Ref 3), Fe-based SMAs have the highest application potential, and two Fe-Mn-Si-based SMA grades have been available, to date, namely Fe-28 Mn-6 Si-5 Cr (Ref 4) and Fe-14 Mn-5 Si-9 Cr-5 Ni (Ref 5) (mass%, as all compositions will be listed hereinafter). Considering that they did not experience reliable two-way shape memory effect (TWSME), Fe-Mn-Si-based SMAs were merely employed for constrained recovery (Ref 6) applications, such as pipe couplings (Ref 7) and fishplates for crane rail fastening (Ref 8). Yet, various attempts were made to develop other types of applications, such as prisms for concrete prestressing (Ref 9), anti-seismic dumpers (Ref 10), and even actuating wires (Ref 11), considering the uncontrolled effects of resistive heating (Ref 12, 13) upon accurate functioning of thermal releasers (Ref 14). On the other hand, promising results were obtained in regards to the pseudoelastic behavior of Fe-based SMAs. Thus, in Fe-Mn-Si, a mechanism was developed to explain the reversion of ε (hexagonal close packed, hcp) stress-induced martensite during cyclic tension-compression loading (Ref 15), while in Fe-Ni-Co SMAs superelastic strains larger than 13% were recently reported (Ref 16).

Classical metallurgical processing of Fe-Mn-Si-Cr-Ni SMAs must overcome a series of difficulties related to compositional segregation (Ref 17), difficult incorporation of Si into melt (Ref 18), Mn loss on melting and heat treatment, which currently occurs in stainless steels (Ref 19), time-consuming chemical composition homogenization (Ref 20), cracking enhancement due to cooling contraction during solidification, and quenching (Ref 21), etc.

One alternative technology, meant to overcome most of inconveniences encountered by classical metallurgical processing, is offered by powder metallurgy (PM) which has already been successfully applied to other SMAs, such as Ti-Ni (Ref 22), Cu-Zn-Al (Ref 23), or Cu-Al-Ni (Ref 24). Moreover, most of the drawbacks in preparing grain-refined microstructures of Fe-Mn-Si-Cr-Ni SMAs with homogenous structure can be eliminated by mechanical alloying (MA) (Ref 25), which is expected to contribute to the increase of solid-state solubility of alloying elements into Fe matrix (Ref 26).

Considering both the above state-of-art technology and the promising results previously reported on the stress-induced formation of martensite in pre-strained (Ref 27) or mechanically cycled (Ref 28) hot-rolled specimens obtained from a powder metallurgy-mechanically alloyed (PM-MA'd) Fe-18Mn-3Si-7Cr-4Ni SMA, the present article aims to reveal

B. Pricop, N.M. Lohan, and **L.G. Bujoreanu**, Faculty of Materials Science and Engineering, The "Gheorghe Asachi" Technical University from Iaşi, Bd. D. Mangeron 61A, 700050 Iasi, Romania; **U. Söyler** and **B. Özkal**, Particulate Materials Laboratory, Metallurgical and Materials Engineering Department, Istanbul Technical University, 34469 Maslak, Istanbul, Turkey; and **D. Chicet** and **C. Munteanu**, Faculty of Mechanical Engineering, The "Gheorghe Asachi" Technical University from Iaşi, Bd. D. Mangeron 61-63, 700050 Iasi, Romania. Contact e-mails: lgbujor@tuiasi.ro.

MA-effects on the thermal behavior of Fe-Mn-Si-Cr-Ni SMA powders subjected to heating up to 773 K, powders which have been used to obtain shape memory rings for constrained-recovery pipe couplings.

2. Experimental Procedure

In a turbula blender, powder mixtures were prepared from commercial powders with nominal composition Fe-14Mn-6Si-9Cr-4Ni. One quarter of the mixture amount was mechanically alloyed (MA'd) for 4 h in SPEXTM D8000 high-energy ball mill, using stainless steel vials and stainless steel milling balls under protective atmosphere, as previously detailed (Ref 29). The powders were studied in two forms: (i) as blended, without MA, further designated as 0_MA, and (ii) as a mixture of as blended and 50% MA'd powders, designated as 50_MA.

The technological flow of processing the constrained recovery rings comprised the following: (i) powder pressing and sintering, (ii) hot rolling, (iii) shape setting, and (iv) thermomechanical training of rings made from both 0_MA and 50_MA specimens. These four stages will be briefly described later.

The powders were pressed and sintered at 1390 K, under cracked ammonia (75% N_2 + 25% H_2) as previously described (Ref 30). The metallographic structures of the two sintered specimens, 0_MA and 50_MA, at macro and microscopic levels, are illustrated in Fig. 1.

By comparing Fig. 1(a) and (b), it is obvious that specimen 50_MA has a smaller volume and is more compact. Both specimens seem to have an austenitic matrix with scarce martensite plates, more numerous at 50_MA specimen, Fig. 1(d).

Hot rolling was performed repeatedly, at 1273 K, with 15% thickness reduction per pass, as previously detailed (Ref 31). The metallographic structures of the two hot-rolled specimens, 0_MA and 50_MA, at macro and microscopic levels, are illustrated in Fig. 2.

It seems that, in spite of compactness-increase caused by rolling, specimen 0_MA still has a higher porosity volume, in Fig. 2(c) as compared to specimen 50_MA, Fig. 2(d).

After hot rolling, the lamellas were machined to straighten the edges and to clean the surfaces, before setting the ring shape, according to the procedure shown in Fig. 3.

Figure3(a) shows that a shape-setting device is used comprising an outer and an inner calibrated tubes. Each lamella, after being heated to approx. 873 K, was mounted between the two calibrated tubes and the assembly was placed into an electric furnace and maintained for 0.9 ks at 1273 K. The resulting shapes are illustrated in Fig. 3(b).

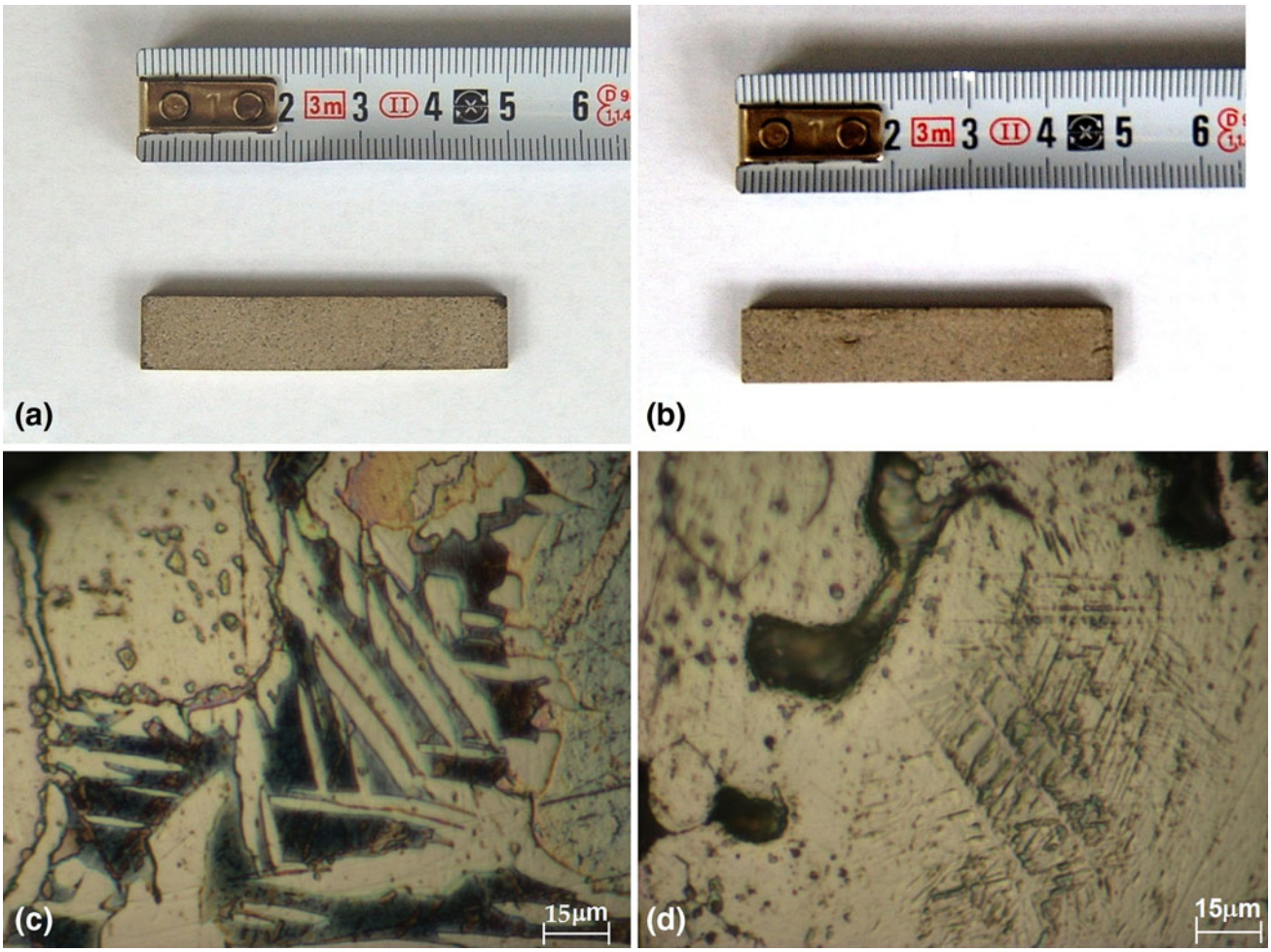

Fig. 1 Structure of as-sintered specimens: (a) macrograph of specimen 0_MA; (b) macrograph of specimen 50_MA; (c) optical micrograph of specimen 0_MA; and (d) optical micrograph of specimen 50_MA

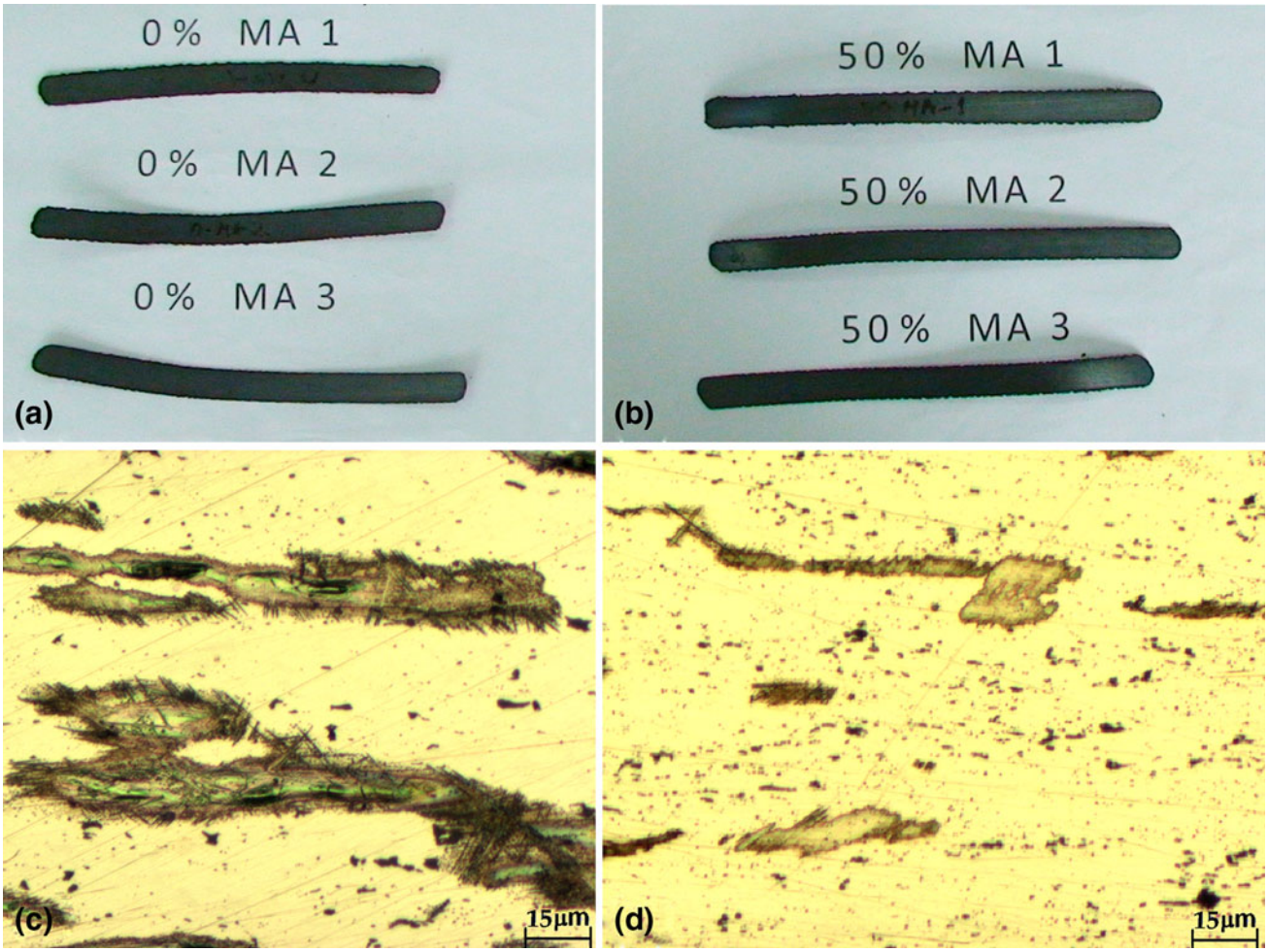

Fig. 2 Structure of hot-rolled specimens: (a) macrograph of specimen 0_MA; (b) macrograph of specimen 50_MA; (c) optical micrograph of specimen 0_MA; and (d) optical micrograph of specimen 50_MA

Finally, the rings were slightly polished, to remove demanganized layer, and trained in bending, after enlarging their diameters at room temperature (RT). The ring shapes succession, accompanying SME occurrence during training, is shown in Fig. 4.

Initially, the enlarged diameter of the rings was $D = 55 \times 10^{-3}$ m, Fig. 4(a). During heating, the diameter progressively decreased, with increasing the temperature, until reaching $D = 47.5 \times 10^{-3}$ m, at 497 K, where an 11.3×10^{-3} m displacement of ring's free end was noticed, Fig. 4(f).

Since the purpose of the present article has been to emphasize the thermal behaviors of 0_MA and 50_MA powders, both powder mixtures were carefully sorted into several samples with initial masses of 40×10^{-6} kg, before being subjected to calorimetric analysis.

Thermal cycles, comprising heating-cooling between RT and 773 K under Ar atmosphere, at a rate of 10 K/min, were applied on a NETZSCH STA 449 F3 device, according to previously mentioned conditions, the results being evaluated with PROTEUS software (Ref 32).

The structural changes of powder mixtures were analyzed by means of a FEI Quanta SEM 200 3D dual beam microscope, with thermal chamber, able to develop both the accelerated electron and focus ion beam (FIB) fascicles and to heat up the specimens under protective atmosphere.

3. Experimental Results and Discussion

The heat flow variations with temperature, recorded during three consecutive heating-cooling cycles applied to the two samples, with 10 K/min between RT and 773 K, are shown in Fig. 5.

The aspects of the exothermic steps observed during heating, as shown in Fig. 5(a) and (c) and of the endothermic steps observed on cooling stages, as shown in Fig. 5(b) and (d) suggest the presence of a reversible solid-state transformation, which could correspond to the ferromagnetic-paramagnetic (F-P) transition of Nickel (Ref 33), the Curie temperature of which lies in this thermal range (Ref 34). With the increasing number of thermal cycles, the critical temperatures of the magnetic transition tend to move to larger values. A summary of DSC data is shown in Table 1. As an effect of combining MA with thermal cycling, it is assumed that Ni atoms diffuse into neighboring particles (such as Fe and Mn), and for this reason, the steps become larger, tend to shift to higher temperatures, and eventually become diffuse and lost (Ref 33). This dispersion is consistent with the anomalous variation of the lattice spacing with temperature, accompanying the F-P transition, which is more pronounced in pure nickel than in nickel alloys (Ref 35). The increased tendency of critical

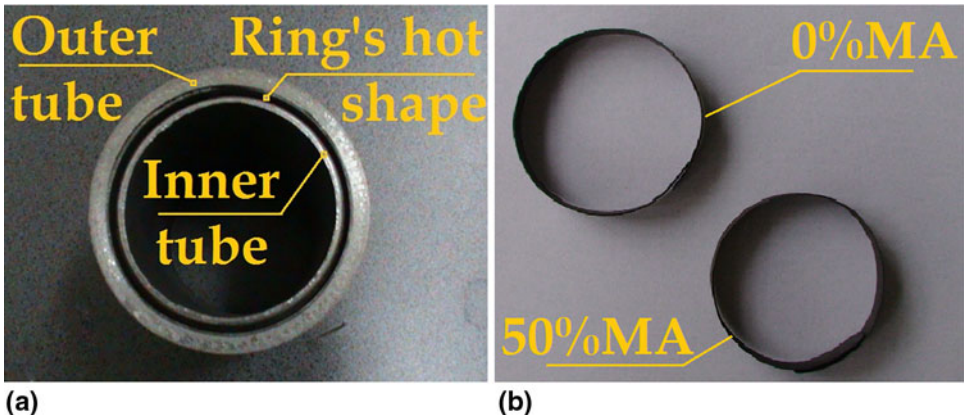

Fig. 3 Processing steps during hot-shape setting of the fastening rings: (a) shape-setting device; and (b) final hot shapes of the rings

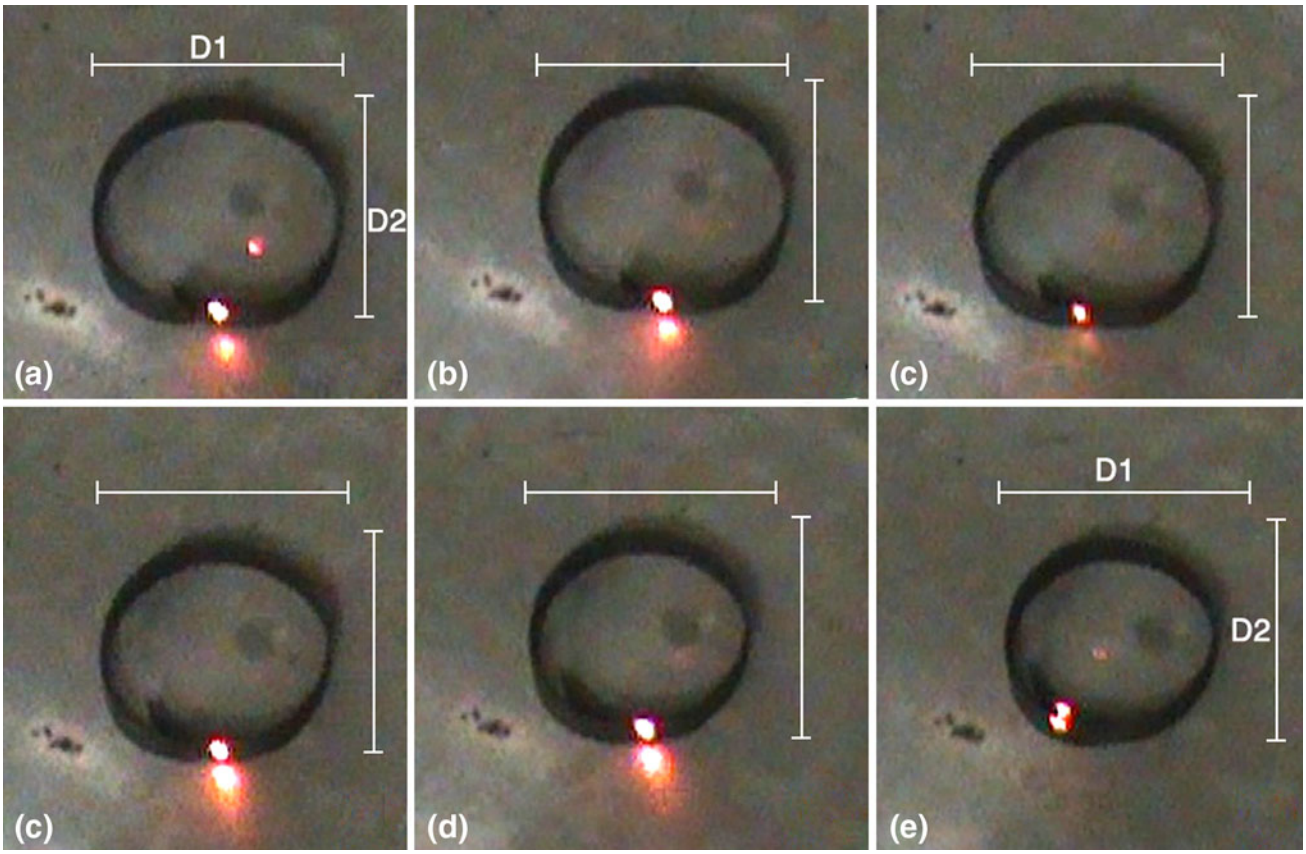

Fig. 4 Successive shapes during thermomechanical training of the rings, described by the values of average diameter, D, and free- end displacement of the ring, d: (a) $D = 55 \times 10^{-3}$m, $d = 0$, at 429 K: (b) $D = 54.7 \times 10^{-3}$m, $d = 0$, at 430 K; (c) $D = 53 \times 10^{-3}$m, $d = 3 \times 10^{-3}$m, at 433 K; (d) $D = 51.7 \times 10^{-3}$m, $d = 6.6 \times 10^{-3}$m, at 446 K; (e) $D = 49.2 \times 10^{-3}$m, $d = 10 \times 10^{-3}$m, at 473 K; and (f) $D = 47.5 \times 10^{-3}$m, $d = 11.3 \times 10^{-3}$m, at 497 K

temperatures for F-P transition is noticeable in Table 1 both with the increasing number of cycles, at the same specimen, and with passing from the as-blended to MA'd-containing powders, in such a way that all the listed temperatures are larger for 50_MA powders as compared to that for 0_MA powders.

Another MA-effect could be indicated by the presence of endothermic venters, seen much more obviously in Fig. 5(c) during 50_MA-heating. Considering that a glass transition is visible in the measurement curve as a step in the endothermic direction (Ref 36), the presence of a certain amount of amorphous phase could be expected in the MA'd fraction of 50_MA Fe-Mn-Si-Cr-Ni powders. Amorphous phases were previously reported in MA'd quintenary Fe-based alloys (Ref 37) even after milling durations of as low as 4 h (Ref 38). Owing to the severe constraints caused by MA processing technique (Ref 39), corroborated with particle refinement and lattice strain enhancement, MA was associated with an increase of the amorphization degree (Ref 40).

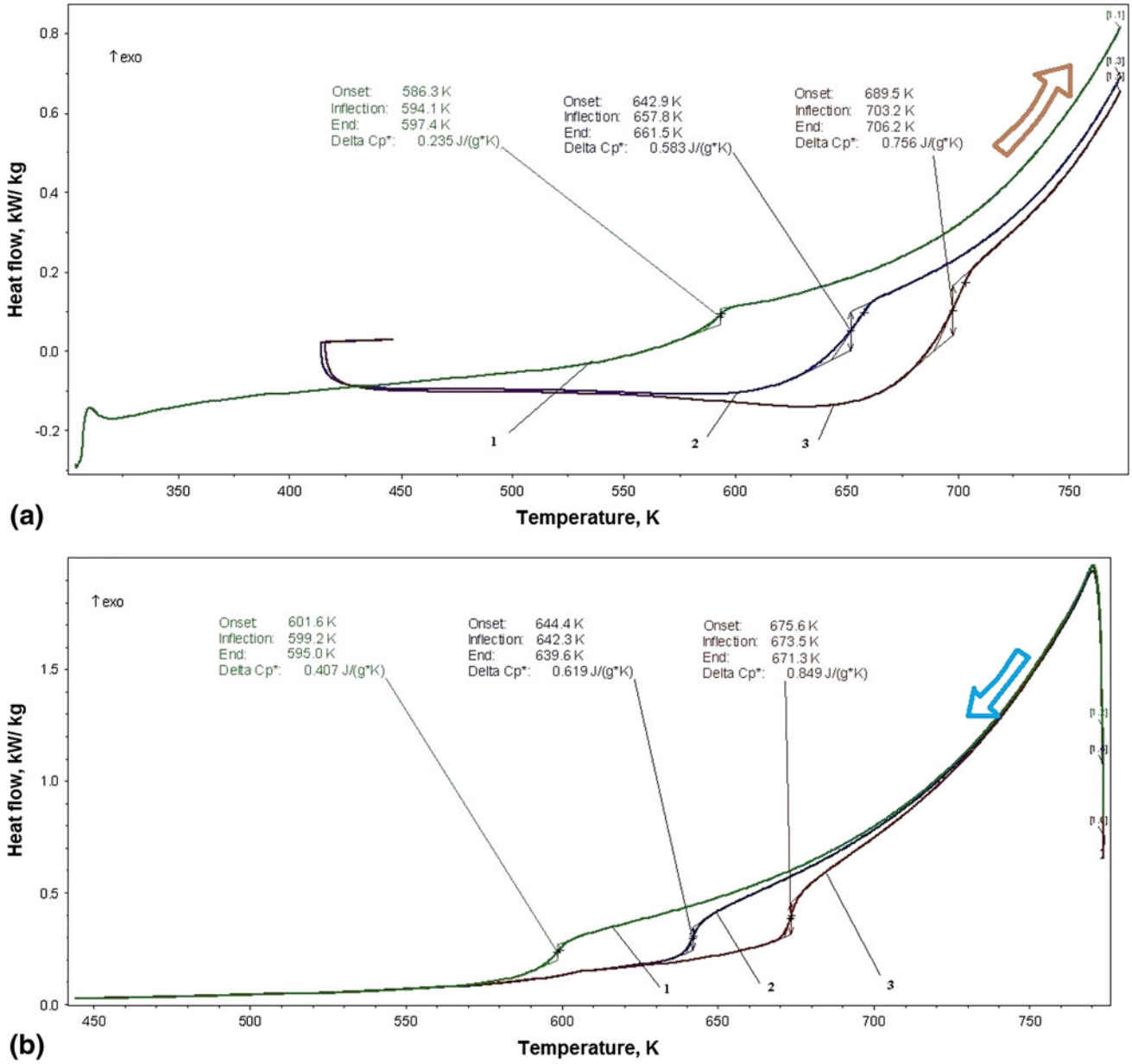

Fig. 5 DSC thermographs recorded during three consecutive thermal cycles performed with a rate of 10 K/ min: (a) 0_MA powders on heating; (b) 0_MA powders on cooling; (c) 50_MA powders on heating; and (d) 50_MA powders on cooling

The structural changes caused by thermal cycling, were analyzed by applying the heating-cooling cycle under protective atmosphere, in the thermal chamber of the dual beam SEM-FIB microscope device. Figure 6 shows typical SEM micrographs of the two powder samples, before and after the heating-cooling cycle.

In Fig. 6(a), the measured average sizes of the elemental particles, in initial as-blended powders, were 50-55 $\times 10^{-6}$ m for Fe, 65-70 $\times 10^{-6}$ m for Mn, 170-230 $\times 10^{-6}$ m for Si, 55-60 $\times 10^{-6}$ m for Cr, and less than 20 $\times 10^{-6}$ m for Ni. After a heating-cooling cycle, Fig. 6(b) illustrates that the general aspect of the powder mixture remained almost the same yet that the surface aspect of the Fe particles has changed, as it will be shown later. As seen from Fig. 6(c), it is impossible to make the difference between the as-blended and the MA'd fractions of 50_MA sample, in initial condition. However, owing to the contribution of MA'd fraction, the average grain size of the powders decreased to 45-50 $\times 10^{-6}$ m. Figure 6(d) shows a representative SEM micrograph of 50_MA powders after a heating-cooling cycle. In this case, as well, the general structural aspect of the powder mixture did not drastically change but very small particles, with average size of 3×10^{-6} m, which were identified as belonging to MA'd fraction, were found partially incorporated into the larger Fe grains, the surface of which have drastically changed.

For a better visualization of these thermal-cycling-induced changes, large magnification SEM micrographs are shown in Fig. 7, illustrating Fe grains belonging to the two powder mixtures after being subjected to a heating-cooling cycle.

In both micrographs, white cilia-like outgrowths, with micrometer-size lengths, and partially incorporated MA'd particles are visible on the surface of Fe particles. For a better

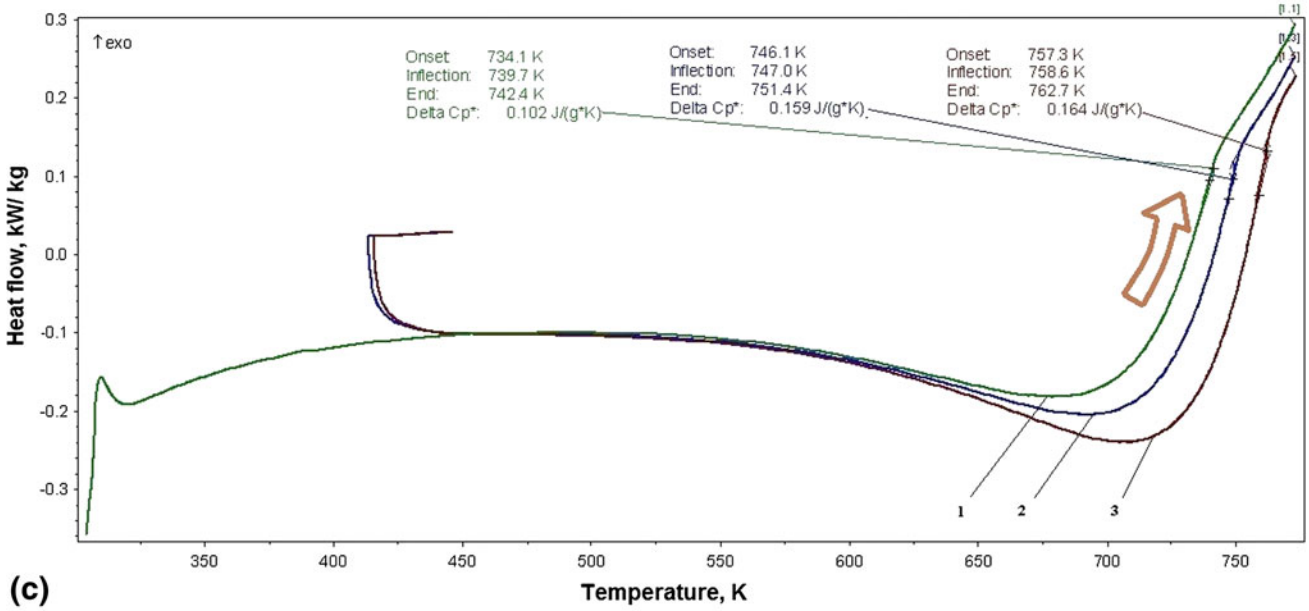

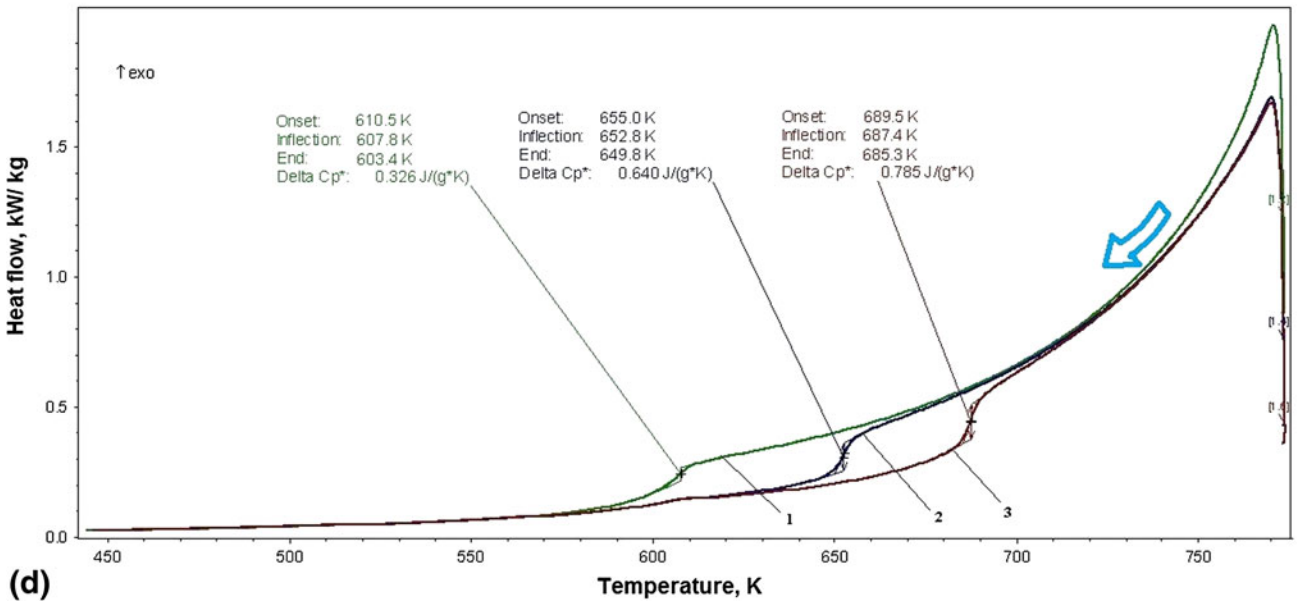

Fig. 5 Continued

Table 1 Summary of calorimetric data from Fig. 5

	Cycle no.	Process	Onset temperature, K	Inflection temperature, K	End temperature, K	Specific heat variation, J/kg K
0% MA	1st	Heating	586.3	594.1	597.4	235
		Cooling	601.6	599.2	595.0	407
	2nd	Heating	642.9	657.8	661.5	583
		Cooling	644.4	642.3	639.6	619
	3rd	Heating	689.5	703.2	706.2	756
		Cooling	675.6	673.5	671.3	849
50% MA	1st	Heating	734.1	739.7	742.4	102
		Cooling	610.5	607.8	603.4	326
	2nd	Heating	746.1	747.0	751.4	159
		Cooling	655.0	652.8	649.8	640
	3rd	Heating	757.3	758.6	762.7	164
		Cooling	689.5	687.4	685.3	785

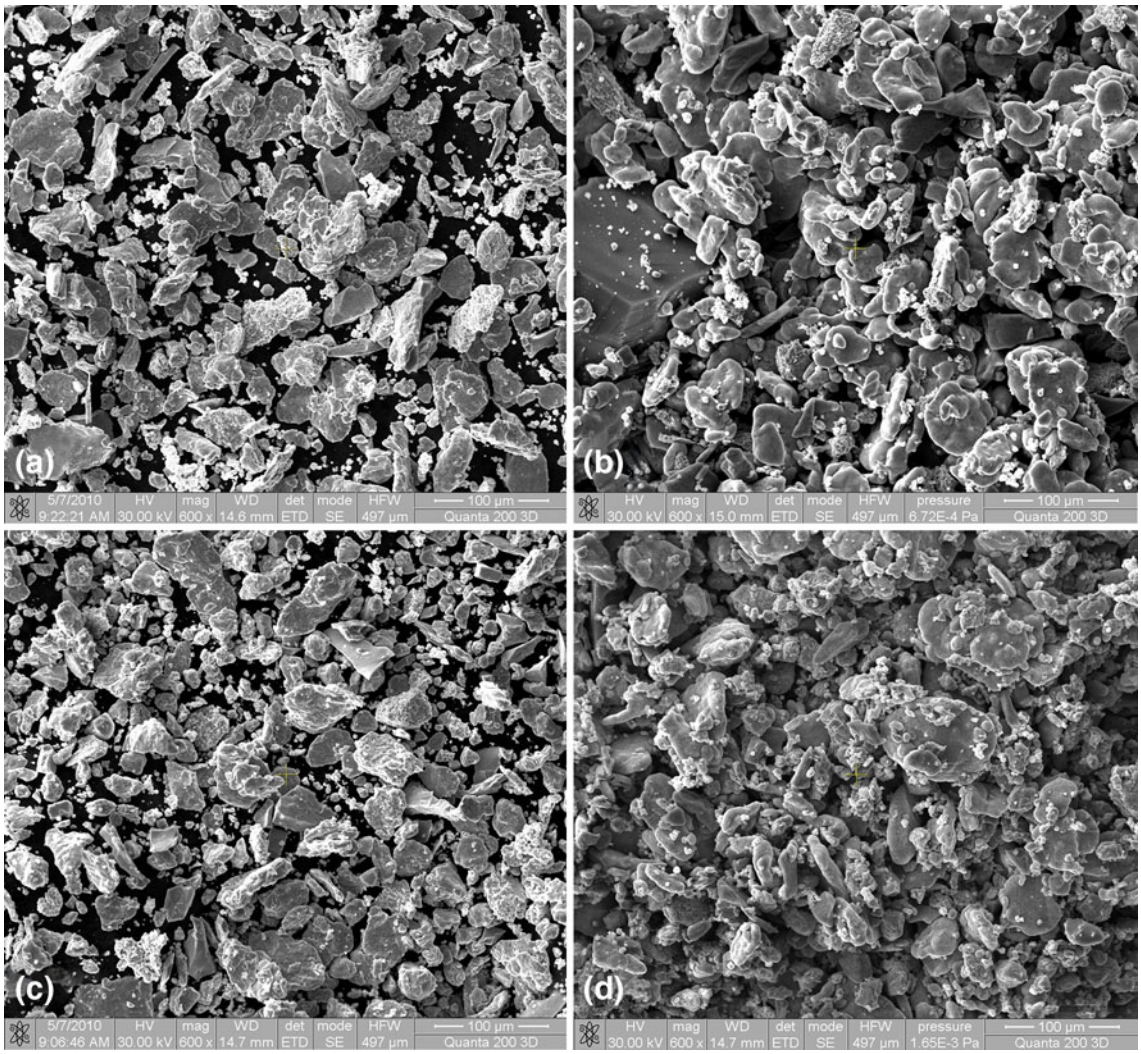

Fig. 6 SEM micrographs : (a) 0_MA powders in initial state; (b) 0_MA after a heating-cooling cycle; (c) 50_MA powders in initial state; and (d) 50_MA after a heating-cooling cycle

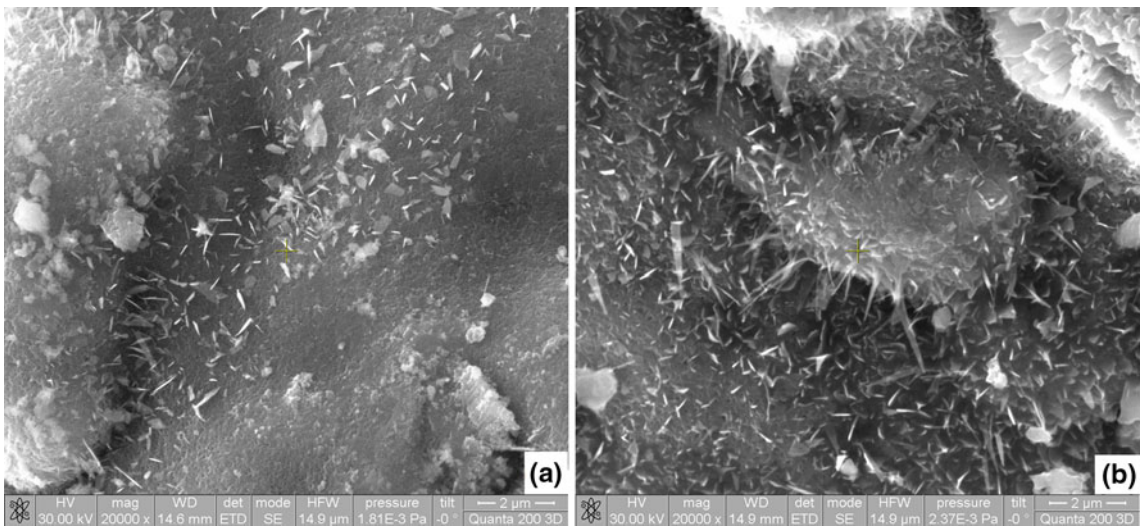

Fig. 7 SEM micrographs, with details observed at the surface of Fe particles, after a heating-cooling cycle to 773 K: (a) 0_MA powders; (b) 50_MA powders

insight on the nature of these thermal-cycling-induced cilia-like outgrowths, a section was cut with FIB and EDX analysis was performed, as emphasized in Fig. 8.

The variation of oxygen content can be observed on right-hand insets, both in MA'd particle and at different levels of the Fe particle. Thus, average oxygen content was 1.5% in MA'd particle and increased from 0.9% in the core to 7% at the surface of Fe particle. These results suggest that, in spite of the protective atmosphere provided by the thermal chamber of SEM-FIB microscope, iron oxides were formed as cilia-like outgrowths. It is obvious that oxidation occurred more intensely at the surface of Fe particles than at the surface of MA'd particles. This difference could be ascribed to the presence of amorphous regions, with less crystallinity, which are assumed to exist in the MA'd fraction of 50_MA powders, since amorphous structures are more corrosion resistant than crystalline ones. A more detailed analysis of the oxidation phenomenon, in MA'd powders was previously performed by TG (Ref 41).

Finally, XRD measurements were performed, aiming to confirm the assumed structural changes which were ascribed to the contribution of the MA'd fraction. For this purpose Fig. 9 shows the XRD patterns of 0_MA and 50_MA samples in initial condition. It is obvious that, at 50_MA sample, there was a diminution of Ni and Si peaks, while some of the Fe peaks became more rounded. This proves the presence of an amorphous phase in MA'd fraction, associated with a certain decrease of the crystallinity degree.

After a heating-cooling cycle, Fig. 10 shows that 0_MA sample did not experience any noticeable structural changes. Conversely, at 50_MA sample, most of the diffraction maxima became sharper and two maxima became apparent as an effect of thermal cycling: (i) the Si maximum located at $2\theta \approx 30°$, and (ii) the Fe maximum located at $2\theta \approx 65°$. This proves that the assumed MA'd fraction partially crystallized during heating, thus contributing to the increase of the crystallinity degree.

4. Conclusions

In powder mixtures of the as-blended and the MA'd particles with nominal composition Fe-14Mn-6Si-9Cr-5Ni (mass%). three phenomena were observed during thermal cycling:

(i) A magnetic transition of Ni, the critical temperatures of which tend to increase with the number of cycles

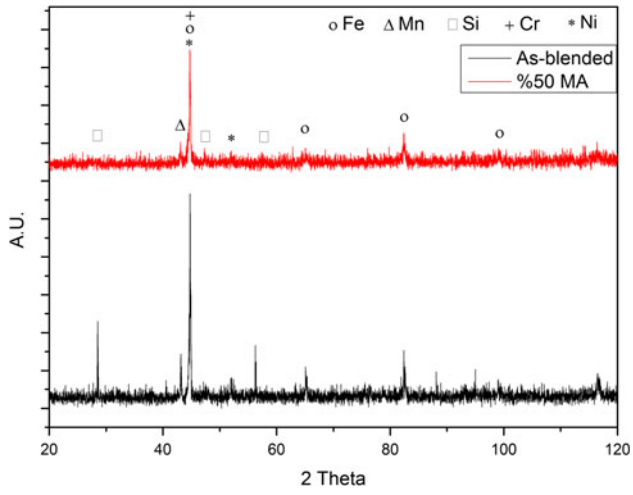

Fig. 9 XRD patterns of 0_MA (as-blended) and 50_MA samples in initial state

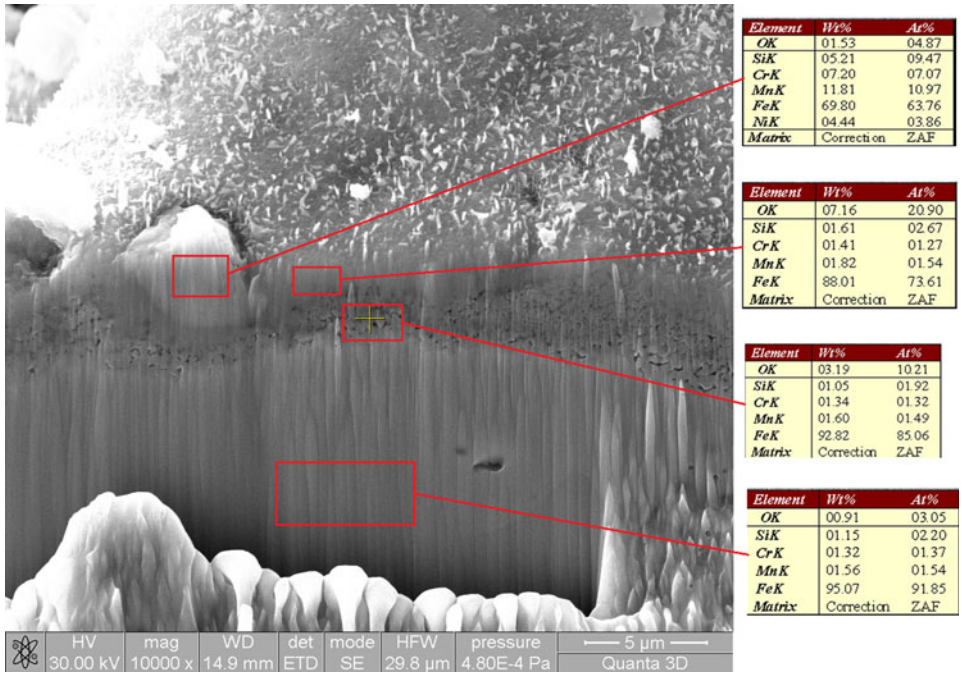

Fig. 8 SEM-FIB micrograph revealing the decrease of oxygen level from the surface to the core of a Fe powder grain with incorporated MA'd particle, within 50_MA powder sample after a heating-cooling cycle to 773 K

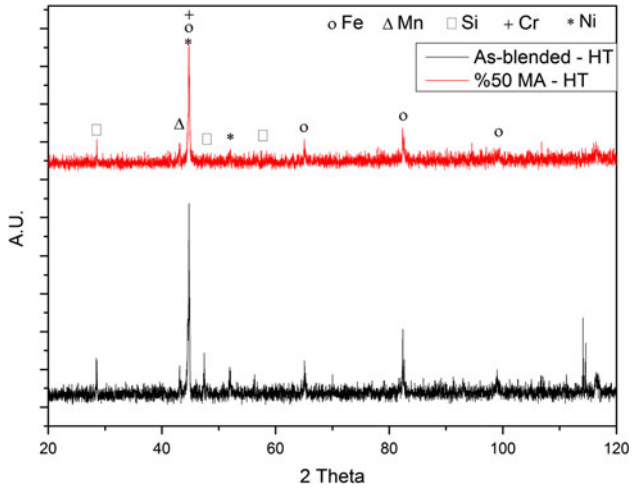

Fig. 10 XRD patterns of 0_MA and 50_MA samples, after a heating-cooling cycle to 773 K

because of the formation of solid solutions as a result of Ni atoms migrating from pure Ni powder into pure Fe and Mn powder particles;

(ii) A glass transition of the amorphous regions is present in MA'd powders, which partially crystallized during each heating;

(iii) A surface oxidation, occurring mostly in the as-blended pure Fe particles, in spite of SEM-FIB-protective atmosphere.

Acknowledgment

B. Pricop acknowledges the financial support from the EURODOC project.

References

1. J. Ma and I. Karaman, Expanding the Repertoire of Shape Memory Alloys, *Science*, 2010, **327**, p 1468, doi:10.1126/science.1186766
2. L. Sun, W.M. Huang, Z. Ding, Y. Zhao, C.C. Wang, H. Purnawali, and C. Tang, Materials and Design, doi:10.1016/j.matdes.2011.04.065
3. R.D. James and K.F. Hane, Martensitic Transformations and Shape-Memory Materials, *Acta Mater.*, 2000, **48**, p 197–222
4. H. Otsuka, H. Yamada, T. Maruyama, H. Tanahashi, S. Matsuda, and M. Murakami, Effects of Alloying Additions on Fe-Mn-Si Shape Memory Alloys, *ISIJ Int.*, 1990, **30**, p 674–679
5. Y. Moriya, H. Kimura, S. Ishizaki, S. Hashizume, S. Suzuki, H. Suzuki, and T. Sampei, *J. Phys. III*, 1991, **1**(novembre C4), p 433–437
6. J.L. Proft and T.W. Duerig, The Mechanical Aspects of Constraint Recovery, *Engineering Aspects of Shape Memory Alloys*, T.W. Duerig, K.N. Melton, D. Stöckel, and C.M. Wayman, Ed., Butterworth-Heinemann, London, 1990, p 115–129
7. S. Kajiwara, A.L. Baruj, T. Kikuchi, and N. Shinya, Low-Cost High-Quality Fe-Based Shape Memory Alloys Suitable for Pipe Joints, *Proc. SPIE*, 2003, **5053**, p 251–261
8. T. Maruyama, T. Kurita, S. Kozaki, K. Andou, S. Farjami, and H. Kubo, Innovation in Producing Crane Rail Fishplate Using Fe-Mn-Si-Cr Based Shape Memory Alloy, *Mater. Sci. Technol.*, 2008, **24**(8), p 908–912
9. T. Sawaguchi, T. Kikuchi, K. Ogawa, S. Kajiwara, Y. Ikeo, M. Kojima, and T. Ogawa, Development of Prestressed Concrete Using Fe-Mn-Si-Based Shape Memory Alloys Containing NbC, *Mater Trans.*, 2006, **47**(3), p 580–583
10. T. Sawaguchi, K. Ogawa, and T. Kikuchi, Absorbtion of Seismic Vibration by Fe-Mn-Si-Based Shape Memory Alloys and TRIP/TWIP Steels, SMST-2007, *Proceedings of the International Conference on Shape Memory and Superelastic Technology*, S. Miyazaki, Ed., December 3-5, 2007 (Tsukuba City, Japan), p 637–644
11. L. Janke, C. Czaderski, M. Motavalli, and J. Ruth, Applications of Shape Memory Alloys in Civil Engineering Structures—Overview, Limits and New Ideas, *Mater. Struct.*, 2005, **38**, p 578–592
12. A. Pleşca, A Complete 3D Thermal Model for Fast Fuses, *8th International Conference on Electric Fuses and their Applications*, ICEFA, Clairmond-Ferrand, Blaise Academic Press, France, 2007, p 79–85
13. A. Pleşca, Thermal analysis of fuses and busbar connections at different type of load variations, International Review on Modelling and Simulations (I.RE.MO.S.) 3(5) 1077-1086 (2010)
14. A. Pleşca, Theoretical Aspects Related to Active Force Evaluation in the Case of Electromagnetic Devices, Int. Rev. Model. Simul. (I.RE.MO.S.), 2011, **4**(2) p 668–673
15. T. Sawaguchi, L.-G. Bujoreanu, T. Kikuchi, K. Ogawa, M. Koyama, and M. Murakami, Mechanism of Reversible Transformation-Induced Plasticity of Fe-Mn-Si Shape Memory Alloys, *Scr. Mater.*, 2008, **59**(10), p 826–829
16. Y. Tanaka, Y. Himuro, R. Kainuma, Y. Sutou, T. Omori, and K. Ishida, Ferrous Polycrystalline Shape-Memory Alloy Showing Huge Superelasticity, *Science*, 2010, **327**, p 1488, doi:10.1126/science.1183169
17. J. Nakano and P.J. Jacques, Effects of the Thermodynamic Parameters of the hcp Phase on the Stacking Fault Energy Calculations in the Fe-Mn and Fe-Mn-C Systems, *CALPHAD (Comput. Coupling Phase Diag. Thermochem.)*, 2010, **34**, p 167–175
18. B.C. Maji and M. Krishnan, Role of Si in Improving the Shape Recovery of FeMnSiCrNi Shape Memory Alloys, *Phys. Procedia*, 2010, **10**, p 111–116
19. T. Matsumiya, Steelmaking Technology for a Sustainable Society, *CALPHAD* (Comput. Coupling Phase Diag. Thermochem.), 2011, doi:10.1016/j.calphad.2011.02.009
20. T. Kirindi, E. Güler, and M. Dikici, Effects of Homogenization Time on the Both Martensitic Transformations and Mechanical Properties of Fe-Mn-Si-Cr-Ni Shape Memory Alloy, *J. Alloys Compd.*, 2007, **433**, p 202–206
21. H. Berns and W. Theisen, *Ferrous Materials. Steel and Cast Iron*, Springer, Berlin, 2008, p 190–207
22. K. Otsuka and X. Ren, Physical Metallurgy of Ti-Ni-Based Shape Memory Alloys, *Prog. Mater. Sci.*, 2005, **50**(5), p 511–678
23. K. Shin, C.R. Wong, and S.H. Whang, Fabrication and Damping Capacity of Cu-Zn-Al Matrix Composites Processed by Powder Metallurgy Route, *Mater. Sci. Eng. A*, 1993, **165**(1), p 35–43
24. Y-T. Choi and I-S. Chung, Production of Cu-Ni-Al Shape Memory Alloys (SMA) by Powder Metallurgy, Metal Powder Report, 1991, **46**(5), p 72
25. Q. He, C. Jia, and J. Meng, Influence of Iron Powder Particle Size on the Microstructure and Properties of Fe_3Al Intermetallics Prepared by Mechanical Alloying and Spark Plasma Sintering, *Mater. Sci. Eng. A*, 2006, **428**(1-2), p 314–318
26. A. Hightower, B. Fultz, and R.C. Bowman, Jr., Mechanical Alloying of Fe and Mg, *J. Alloy Compd.*, 1997, **252**(1-2), p 238–244
27. L.G. Bujoreanu, S. Stanciu, B. Özkal, R.I. Comăneci, and M. Meyer, Comparative Study of the Structures of Fe-Mn-Si-Cr-Ni Shape Memory Alloys Obtained by Classical and by Powder Metallurgy, Respectively, *ESOMAT*, 2009, **2009**, p 05003
28. B. Pricop, U. Söyler, R.I. Comăneci, B. Özkal, and L.G. Bujoreanu, Mechanical Cycling Effects at Fe-Mn-Si-Cr-Ni SMAs Obtained by Powder Metallurgy, *Phys. Procedia*, 2010, **10**, p 125–131
29. A.U. Söyler, B. Özkal, and L.G. Bujoreanu, Sintering Densification and Microstructural Characterization of Mechanical Alloyed Fe-Mn-Si Based Powder Metal System, *TMS Suppl. Proc.*, 2010, **3**, p 785–792
30. A.U. Söyler, B. Özkal, and L.G. Bujoreanu, Investigation of Mechanical Alloying Process Parameters on Fe-Mn-Si Based System, *TMS Suppl. Proc.*, 2011, **1**, p 577–583
31. L.G. Bujoreanu, V. Dia, S. Stanciu, M. Susan, and C. Baciu, Study of Tensile Constrained Recovery Behavior of a Fe-Mn-Si Shape Memory Alloy, *Eur. Phys. J. (Special Topics)*, 2008, **158**(May), p 15–20
32. L.G. Bujoreanu, S. Stanciu, R.I. Comăneci, M. Meyer, V. Dia, and C. Lohan, Factors Influencing the Reversion of Stress-Induced Martensite to Austenite in a Fe-Mn-Si-Cr-Ni Shape Memory Alloy, *J. Mater. Eng. Perform.*, 2009, **18**, p 500–505
33. A.S. Bolokang and M.J. Phasha, Thermal Analysis on the Curie Temperature of Nanocrystalline Ni Produced by Ball Milling, Adv. Powder Technol., 2010, doi:10.1016/j.apt.2010.07.005

34. W. Xiong, H. Zhang, L. Vitos, and M. Selleby, Magnetic Phase Diagram of the Fe-Ni System, *Acta Mater.*, 2011, **59**, p 521–530
35. T.B. Massalski, Structure and Stability of Alloys, *Physical Metallurgy*, vol. I, R.W. Cahn, P. Haasen, Ed., North-Holland, Amsterdam, 1996, p 35–204
36. http://www.tainst.com, Thermal Analysis Application Brief Detection of the Glass Transition in Metal Glasses by Differential Scanning Calorimetry (DSC) and Dynamic Mechanical Analysis (DMA), TA 137A
37. C. Suryanarayana and S. Sharma, Glass Formation in Mechanically Alloyed Fe-Based Systems, *Funct. Mater. Lett.*, 2009, **2**(4), p 147–155
38. J. Bhatt and B.S. Murty, On the Conditions for the Synthesis of Bulk Metallic Glasses by Mechanical Alloying, *J. Alloy Compd.*, 2008, **459**, p 135–141
39. C. Suryanarayana, E. Ivanov, and V.V. Boldyrev, The Science and Technology of Mechanical Alloying, *Mater. Sci. Eng. A*, 2001, **304-306**, p 151–158
40. U. Patil, S.-J. Hong, and C. Suryanarayana, An Unusual Phase Transformation During Mechanical Alloying of an Fe-Based Bulk Metallic Glass Composition, *J. Alloy Compd.*, 2005, **389**, p 121–126
41. B. Pricop, U. Söyler, N.M. Lohan, B. Özkal, D. Chicet, A. David, and L.-G. Bujoreanu, Mechanical Alloying Effects on the Thermal Behaviour of a Fe-Mn-Si-Cr-Ni Shape Memory Alloy Under Powder Form, *Optoelectron. Adv. Mater.*, 2011, **5**(5), p 555–561